

**PPP:  
A GATE-LEVEL POWER SIMULATOR  
A WORLD WIDE WEB APPLICATION**

**Alessandro Bogliolo  
Luca Benini  
Giovanni De Micheli  
Bruno Riccò**

Technical Report: CSL-TR-96-691

March 1996

This work was partially supported by NSF (under contract MIP-9421129)  
and by AEI (under grant De Castro)



# PPP: A Gate-Level Power Simulator A World Wide Web Application

Alessandro Bogliolo   Luca Benini   Giovanni De Micheli   Bruno Riccò<sup>1</sup>

Technical Report: CSL-TR-96-691

March 1996

Computer Systems Laboratory  
Departments of Electrical Engineering and Computer Science  
Stanford University  
Stanford, CA 94305-9040

## Abstract

Power consumption is an increasingly important constraint for complex ICs. Accurate and efficient power estimations are required at any level of abstraction to steer the design process.

PPP is a Web-based integrated environment for synthesis and simulation of low-power CMOS circuits. We describe the simulation engine of PPP and we propose a new paradigm for tool integration.

The simulation engine of PPP is a gate-level simulator that achieves accuracy comparable with electrical simulation, while keeping performance competitive with traditional gate-level techniques. This is done by using advanced symbolic models of the basic library cells, that exploit the understanding of the main phenomena involved in power consumption. In order to maintain full compatibility with gate-level design tools, we use VERILOG-XL as simulation platform. The accuracy obtained on benchmark circuits is always within 6% from SPICE also for single-gate/single-pattern power analysis, thus providing the local information needed to optimize the design.

Interface and tool integration issues have been addressed using a Web-based approach. The graphical interface of PPP is a dynamically generated tree of interactive HTML pages that allow the user to access and execute the tool through the Internet by using his/her own Web-browser. No software installation is required and all the details of data transfer and tool communication are hidden to the user.

**Key Words and Phrases:** Power consumption, Symbolic gate model, Gate-level simulation, CAD tool integration, Web-based application

---

<sup>1</sup>With the DEIS, University of Bologna, viale Risorgimento 2, 40135 Bologna, Italy.

Copyright ©1996

Alessandro Bogliolo, Luca Benini, Giovanni De Micheli and Bruno Riccò

# Contents

<b>1</b>	<b>Introduction</b>	<b>1</b>
<b>2</b>	<b>Gate-Level Power Simulation</b>	<b>2</b>
2.1	Cell-Based Power Simulation . . . . .	3
<b>3</b>	<b>A New Approach</b>	<b>5</b>
3.1	Basic Idea . . . . .	5
3.2	Advanced Gate Models . . . . .	6
3.3	Evaluating $E_c$ . . . . .	6
3.4	Evaluating $E_w$ . . . . .	8
3.5	Multiple Transitions . . . . .	8
3.6	Timing Information . . . . .	10
3.7	Sequential Elements . . . . .	11
3.7.1	Static Sequential Elements . . . . .	11
3.7.2	Dynamic Elements . . . . .	12
3.8	Implementation . . . . .	13
<b>4</b>	<b>Web-Based Tool Development</b>	<b>13</b>
4.1	Motivations and Background . . . . .	13
4.2	The PPP Paradigm . . . . .	14
<b>5</b>	<b>Tool Architecture</b>	<b>16</b>
5.1	Application Layer . . . . .	16
5.2	Communication Layer . . . . .	17
5.3	Interface Layer . . . . .	18
5.4	Bandwidth management . . . . .	18
5.5	Implementation Details . . . . .	19
<b>6</b>	<b>PPP User Session</b>	<b>20</b>
6.1	Circuit Specification and Mapping . . . . .	21
6.2	Simulation Setup . . . . .	22
6.3	Power Simulation . . . . .	24
<b>7</b>	<b>Experimental Results</b>	<b>25</b>
<b>8</b>	<b>Conclusions and Future Work</b>	<b>27</b>
<b>9</b>	<b>Acknowledgements</b>	<b>28</b>



## 1 Introduction

Power dissipation in VLSI systems has recently become a critical metric for design evaluation. A large number of power estimation techniques have been recently proposed [1, 2, 3, 4], based on models at different levels of abstraction, ranging from electrical level to architectural level [5, 6, 7]. Electrical-level simulators produce the most accurate results, but are often very demanding in terms of computational resources. Moreover, the large number of simulations needed to reach a reliable estimate of average power dissipation further restricts the class of circuits that can be analyzed with electrical simulators in a reasonable time.

At a higher level of abstraction, logic-level simulation allows power estimation for very large blocks, often enabling full-chip simulation. As a consequence, for CMOS digital circuits, logic-level simulation is usually the preferred tool for validation and debugging, and the large majority of designers is highly familiar with logic simulation tools. Mainly for these reasons, many attempts have been made to provide power estimation at the logic level. In the simplest model, power is estimated observing the *switching activity* at the output of the basic logic blocks of the circuit (weighted by the load capacitance). The advantage of this model is that it enables the application of *pattern independent* techniques, which provide an estimate of the average switching activity without actually simulating the circuit with a large number of test patterns [2].

Power estimation based on switching activity has however limited accuracy, mainly because it does not consider phenomena such as non-instantaneous signal transitions, spurious transitions (glitches) and gate internal capacitances, that may have a sizable impact on the total power dissipation. In order to overcome these difficulties, advanced logic simulation techniques have been proposed that allow increased accuracy, while maintaining the abstraction at the logic level [8, 9, 10]. In these approaches, lookup tables are obtained by electrical simulation of the basic building blocks, and the collected data are then used during gate-level simulation.

Although these techniques reported promising results, they have two main limitations. First, they do not assume any model for the internal structure of the basic building blocks (*gates*). Second, they do not deal with multiple input transitions that are not perfectly aligned in time, with misalignments smaller than the propagation delay of the gate. In this work we propose a more accurate model based on the structure of the gate (and on the physical understanding of the electrical phenomena involved in power dissipation) that overcomes the limitations above mentioned, while keeping computational efficiency competitive with traditional gate-level power simulation.

Our technique exploits a BDD-based symbolic model for describing the charge and discharge of parasitic (and load) capacitances and the flow of short circuit current. Lookup tables are used only for modeling the timing behavior of the circuit (as it is commonly done in full-delay simulation), therefore power simulation only marginally increases the memory usage. Our model is flexible and can be used to accurately estimate power dissipation for gates in a large range of

load and input conditions. As a result, our method is highly accurate also for single gate (*local*) power estimate, allowing the individuation of critical gates during design optimization.

We have implemented our algorithms using VERILOG-XL as simulation platform, therefore maintaining full compatibility with design environments based on VERILOG HDL. For our test library the accuracy on local power estimation is within 6% from SPICE under a wide range of fan-in and fan-out conditions, while the accuracy on the average power dissipation for large benchmarks is even higher. The speed penalty with respect to unit-delay VERILOG simulation is within a factor of 6, while the speedup with respect to fast SPICE simulation ranges from two to three orders of magnitude.

We have used our simulator as the starting point for the development of a CAD tool that we called PPP. PPP has been conceived as an integrated environment for simulation and synthesis of low-power CMOS circuits. Its main features are modularity, machine independence, resource distribution and remote execution. All these features are implemented by following a new tool integration and interfacing paradigm based on the World Wide Web. The graphical interface of PPP is a net of interactive HTML pages that can be accessed through the Internet using traditional Web-browsers.

In the next section we discuss the main issues involved in gate-level power simulation. In section 3 we introduce our model of power consumption in CMOS gates and we describe how to use it in an event-driven simulation context. In section 4 we introduce the PPP-paradigm for Web-based tool integration and interfacing. The architecture of PPP is then described in section 5 and a typical user session is exemplified in section 6. In section 7 we report the experimental results obtained on a large set of benchmark circuits and in section 8 we draw conclusions.

## 2 Gate-Level Power Simulation

Traditional gate-level power estimates are based on the simplifying assumption that the supply current required by a CMOS circuit is essentially spent on charging load capacitances at the outputs of the switching gates. Because of this assumption, the inner structure of the gates is neglected and the average power consumption is evaluated simply by looking at the switching activity (toggle count) and the capacitive load at the gate outputs.

In this way, however, the actual power consumption can be heavily underestimated since several parasitic phenomena (such as short-circuit currents, charging and discharging of internal capacitances and charge sharing) that may have a sizable impact on the global power, cannot be captured.

**Example 1** *Fig. 1 represents a CMOS realization of a three inputs OR gate. Starting from the input configuration  $\mathbf{x} = 100$ , consider a transition of the input signal  $x_1$  from 1 to 0 (boldfacing is hereafter used to denote Boolean vectors:  $\mathbf{x} = [x_1 x_2 x_3]$ ). The only effect of this transition that can be captured at logic level is the discharging of  $C_L$ , that does not cause any current from power*



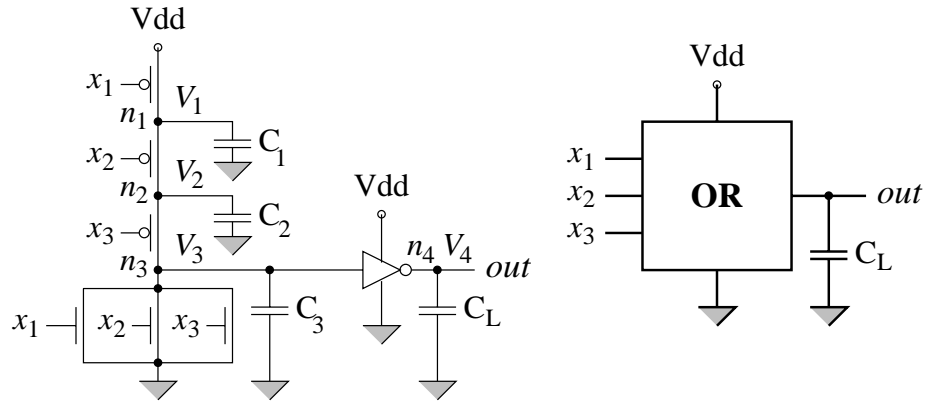


Figure 1: CMOS realization of a three input OR gate. Parasitics are modeled by means of four constant capacitors to ground:  $C_1 = C_2 = 11\text{fF}$ ,  $C_3 = 157\text{fF}$  and  $C_L = 136\text{fF}$ .

supply. However, a sizable power is actually drawn by the gate due to the charging of internal capacitances and to the presence of transient conductive paths from power-supply to ground. In particular, the power consumption is of  $0.22\text{mW}$  (according to HSPICE) for an input transition of  $0.1\text{ns}$  and a clock period of  $20\text{ns}$ . This is of the same order of the supply power required for a rising transition of the output node, even with an additional load of  $50\text{fF}$ .  $\square$

Moreover, spurious transitions (glitches) that may represent the 20% of the switching activity [11], cannot be accurately accounted for, due to the use of simplified cell delay models.

**Example 2** At a logic level of abstraction, changing the inputs of the OR gate of Fig. 1 from  $\mathbf{x} = 100$  to  $\mathbf{x} = 010$  does not cause any effect. However, a misalignment between the falling and rising edges of input signals  $x_1$  and  $x_2$  (i.e.,  $x_2$  rising  $0.4\text{ns}$  after  $x_1$  has fallen), may give rise to a power consumption of  $0.08\text{mW}$  (according to HSPICE), because of two phenomena (see Fig. 1):

- i) a double, spurious transition (glitch) at the output node, causing the charging/discharging of both  $C_L$  and  $C_3$ , and
- ii) short-circuit currents through both the CMOS stages.  $\square$

In principle, the above mentioned limitations can be overcome by taking advantage, during gate-level simulation, of previously collected information about the basic building blocks of the circuit.

## 2.1 Cell-Based Power Simulation

Cell-based power estimation [8] improves upon simple logic-level estimation and consists of the two steps paradigm of cell characterization and logic simulation. The characterization phase includes a set of electrical simulations of each library-cell for all possible input transitions and

for a wide range of fan-in and fan-out conditions. Timing and power information obtained in this way is used to construct lookup tables for each library-cell.

Logic simulation is then performed by a back-annotated event-driven simulator. Whenever a transition occurs at the input of a gate, both the propagation delay and the energy drawn by the gate are read on the corresponding lookup tables. Notice that during simulation, the gate is seen as a black-box, no information about its internal structure and status is exploited.

In principle, as long as the lookup tables have entries corresponding to the actual fan-in/fan-out conditions of each gate of the circuit, the back-annotated gate-level simulation reaches the accuracy of the electrical one. However, the power consumption and the propagation delay of library cells cannot be pre-characterized for all possible transitions and for all possible values of parameters they depend on (input slopes and skews, output loads). In practice, instead, electrical simulations are performed only for single input transitions and for a given set of typical values of the I/O parameters, thus reducing both the number of electrical simulations and the size of the lookup tables. The subsequent discretization ultimately impairs the accuracy of the power estimate. On the other hand, the results of electrical simulations are not accurately fit by any elementary algebraic function of input patterns and I/O parameters.

Moreover, the power consumption of a CMOS cell actually depends on the charge status of its internal capacitances, that is usually neglected in the context of gate-level simulation, giving rise to further approximations.

**Example 3** *With respect to Fig. 1, consider a transition from  $\mathbf{x} = 101$  to  $\mathbf{x} = 001$ . The actual energy drawn by the OR gate corresponding to this input transition depends on the charge status of its internal capacitances. In particular, no supply energy is required if both  $C_1$  and  $C_2$  have already been charged at  $V_{dd}$  by a previously applied input vector  $\mathbf{x} = 001$ , while otherwise  $0.44\text{pJ}$  ( $22\mu\text{W}$  with a  $20\text{ns}$  cycle-time) are dissipated. Hence, internal voltages should also be taken into account in order to obtain accurate power estimates.  $\square$*

Recently, more refined methods have been proposed that partially exploit the knowledge of the power consuming phenomena inside the cells. In [10] it is observed that the power dissipated by a cell is characterized by two radically different behaviors depending on the ratio between slope of the input and output transitions. If the ratio is larger than one, short circuit current becomes important, while if it is smaller this contribution is less relevant. Based on this observation, a model is proposed in which two different fitting formulas are used depending on the above mentioned ratio. The accuracy in this approach is limited by the simple analytic model and the by lack of information on the internal state of the cells.

In [9] a finite-state machine (FSM) model for the cell is proposed, in which the internal charge status of the gate is modeled, and the power dissipated during input transitions is represented by weights associated with the state transitions of the FSM. However, the power dissipated during a transition depends not only on the initial and final charge status, but also on the capacitive load

and on the slope of input and output transitions. This dependency is not explicitly modeled, thus requiring the use of (large) lookup tables associated with each transition.

Moreover, both techniques do not model accurately signal waveforms, multiple misaligned input transitions and parasitic phenomena causing intermediate voltage levels (such as signal glitches and charge sharing). In the next section, we present a new cell-based approach that overcomes the above limitations.

### 3 A New Approach

As mentioned before, cell-based power estimation techniques must compromise between the size of the lookup tables and the accuracy of the estimates. In order to obtain a better trade-off between efficiency and accuracy, we use an advanced model of power consumption in CMOS cells, based on the understanding of the electrical phenomena involved.

#### 3.1 Basic Idea

In principle, the supply current  $I(t)$  drawn by a CMOS cell corresponding to an input transition (namely, from  $\mathbf{x}^i$  to  $\mathbf{x}^f$ ) can be viewed as consisting of two contributions:

- a **charging** current  $I_c(t)$ , that increases the total charge of internal and load capacitors, and
- a **wasted** current  $I_w(t)$ , that does not affect the charge status of the cell.

The energy drawn by the cell during the whole transition can accordingly be partitioned into two contributions:

$$E_c = \int_{t^i}^{t^f} V_{dd} I_c(t) dt, \quad E_w = \int_{t^i}^{t^f} V_{dd} I_w(t) dt.$$

Apexes  $i$  and  $f$  are hereafter used to denote the beginning and the end of a given transition, respectively.

In general, even if we run accurate electrical simulations, we cannot distinguish between the two portions of supply current ( $I_c$  and  $I_w$ ). However, we can evaluate  $E_c$  simply by looking at the charge status of the cell. In fact, since  $I = \frac{dq}{dt}$ ,  $E_c$  can be expressed as

$$E_c = V_{dd} \int_{t^i}^{t^f} I_c(t) dt = V_{dd} \Delta Q, \quad (1)$$

where  $\Delta Q$  is the total charge provided by  $V_{dd}$  to internal and load capacitors.  $\Delta Q$  can therefore be computed by the following equation:

$$\Delta Q = \sum_{j \in \mathcal{S}} \Delta q_j, \quad (2)$$

where  $\mathcal{S}$  is the set of connected nodes with a connection to  $V_{dd}$  for input vector  $\mathbf{x}^j$ , and  $\Delta q_i$  is the charge increase at node  $n_i$ :  $\Delta q_j = C_j(V_j^f - V_j^i)$ . It is worth noting that  $E_c$  does NOT depend on the I/O parameters, and its computation ultimately requires only the knowledge of the charge status (or voltage level) at each node of the cell.

The wasted energy ( $E_w = E - E_c$ ), on the other hand, does NOT depend on the internal charge status, and can be approximated by a (linear) function of the I/O parameters, obtained by fitting the results of electrical simulations.

### 3.2 Advanced Gate Models

For each cell, we provide the layout-extracted internal capacitances and we model the parasitics with constant capacitors to ground, as shown in Fig. 1. We denote by  $\mathcal{N}$  the ordered set of cell nodes  $(n_1, n_2, \dots, n_N)$ , including primary outputs, and by  $C_i$  the capacitance between node  $n_i$  and ground.

In order to compute  $E_c$ , we need to know the voltage level at each node at the beginning and at the end of any transition. Moreover, we need to dynamically determine the set ( $\mathcal{S}$ ) of nodes connected to power supply. To solve these problems, we keep track of the Boolean conditions enabling the connection of each node to ground ( $V_{ss}$ ), to  $V_{dd}$  and to each other node in the cell.

These conditions make up a **connection matrix**  $\mathcal{M}(\mathbf{x})$ , with  $N$  rows and  $N$  columns associated with the cell nodes: entry  $m_{i,j}(\mathbf{x})$  of the matrix is a Boolean function of the cell inputs, taking value 1 for those input configurations for which a conductive path exists between nodes  $n_i$  and  $n_j$ . Two additional columns (namely  $N + 1$  and  $N + 2$ ) are used to represent the connectivity to power supply ( $d$ ) and ground ( $s$ ).

**Example 4** For the OR gate of Fig. 1, the elements of the first row of the connection matrix are:  $m_{1,1}(\mathbf{x}) = 1$ ,  $m_{1,2}(\mathbf{x}) = x'_2$ ,  $m_{1,3}(\mathbf{x}) = x'_2 x'_3$ ,  $m_{1,4}(\mathbf{x}) = 0$ ,  $m_{1,d}(\mathbf{x}) = x'_1$ , and  $m_{1,s}(\mathbf{x}) = x_1(x_2 + x_3)$ . The output node is denoted by  $n_4$ .  $\square$

The efficient handling of the connection matrix is obtained by using Reduced Ordered Binary Decision Diagrams (BDDs) to represent Boolean functions [12]. To this purpose notice that the square sub-matrix consisting of the first  $N$  columns of  $\mathcal{M}(\mathbf{x})$  is symmetrical, and the BDD-based representation allows a consistent amount of sharing among its entries.

It is also worth noting that  $\mathcal{M}(\mathbf{x})$  is constructed only once for all, during the characterization phase. At run-time, for each input pattern  $\mathbf{x}$  the connection status is then obtained from  $\mathcal{M}(\mathbf{x})$  in linear time, by simple BDD evaluations.

### 3.3 Evaluating $E_c$

During logic simulation, the connection matrix is used both to compute  $E_c$  and to update the charge status. In particular, the total charge provided by power supply to the internal and load

capacitors can be easily evaluated using the column of  $\mathcal{M}$  associated with  $V_{dd}$ . For a generic cell with  $N$  nodes (including primary output nodes), Equation (2) can be rewritten as:

$$\Delta Q = \sum_{i=1}^N m_{i,d}(\mathbf{x}^f) C_i (V_i^f - V_i^i). \quad (3)$$

**Example 5** *With respect to Fig. 1, the Boolean conditions enabling the connection of each node of the OR gate to power supply are:  $m_{1,d}(\mathbf{x}) = x'_1$ ,  $m_{2,d}(\mathbf{x}) = x'_1 x'_2$ ,  $m_{3,d}(\mathbf{x}) = x'_1 x'_2 x'_3$ ,  $m_{4,d}(\mathbf{x}) = x_1 + x_2 + x_3$ . For instance, the charge provided by  $V_{dd}$  when the cell inputs switch to  $\mathbf{x}^f = 011$  is then expressed by:*

$$\Delta Q = C_1(V_1^f - V_1^i) + C_4(V_4^f - V_4^i),$$

where  $C_4$  corresponds to the output load  $C_L$ .  $\square$

Equation (3) requires the complete knowledge of node voltages at the beginning and at the end of the transition. Node voltages are updated by exploiting the connection matrix:

$$V_i^f = m_{i,d}(\mathbf{x}^f) V_{dd} + m_{i,s}(\mathbf{x}^f) V_{ss} + m_{i,float}(\mathbf{x}^f) \frac{\sum_{j=0}^N m_{i,j}(\mathbf{x}^f) C_j V_j^i}{\sum_{j=0}^N m_{i,j}(\mathbf{x}^f) C_j}, \quad (4)$$

where  $m_{i,float}(\mathbf{x}^f)$  takes value 1 whenever node  $n_i$  is floating:  $m_{i,float} = m'_{i,d} m'_{i,s}$ . In practice,  $m_{i,d}(\mathbf{x})$ ,  $m_{i,s}(\mathbf{x})$  and  $m_{i,float}(\mathbf{x}^f)$  work as mutually exclusive selection functions:

- if  $n_i$  is connected to power supply ( $m_{i,d} = 1$ ), the new value of  $V_i$  is  $V_{dd}$ ;
- if  $n_i$  is connected to ground ( $m_{i,s} = 1$ ), the new value of  $V_i$  is  $V_{ss}$ ;
- if  $n_i$  is floating ( $m_{i,float} = 1$ ), the new value of  $V_i$  is computed by taking into account the charge sharing with other channel-connected nodes.

**Example 6** *Consider a transition to  $\mathbf{x}^f = 101$  at the inputs to the OR gate of Fig. 1. At the end of the transition, node  $n_1$  is floating and connected only to  $n_2$ . So, the new value of  $V_1$  is given by the charge sharing between  $n_1$  and  $n_2$ :*

$$V_1^f = \frac{C_1 V_1^i + C_2 V_2^i}{C_1 + C_2}.$$

$\square$

Notice that Equation (4) also allows us to take implicitly into account the effect of threshold drop on the voltage levels of internal nodes connected to  $V_{dd}$  ( $V_{ss}$ ) through n-channel (p-channel) transistors [13]. For a generic node (say,  $n_i$ ) this is done simply by replacing the nominal values of  $V_{dd}$  and  $V_{ss}$ , with values obtained from electrical simulations (namely,  $V_{dd_i}$  and  $V_{ss_i}$ ) taking into account transistor threshold drops.

The main source of error in our estimation of  $E_c$  is then the constant capacitor to ground model (floating capacitors are modeled as capacitors to ground). The effect of nonlinear time-varying junction capacitances and feedthrough parasitic capacitances are approximatively accounted for in the  $E_w$  component of energy dissipation.

### 3.4 Evaluating $E_w$

The main contribution to  $E_w$  is due to the presence of short circuit currents from power supply to ground. The connection matrix can be used to detect conditions for which there is a transient open path between  $V_{dd}$  and  $V_{ss}$ . In practice, a wasted current is drawn from power supply whenever a node that was connected to  $V_{dd}$  for input vector  $\mathbf{x}^i$  is connected to  $V_{ss}$  for input vector  $\mathbf{x}^f$ , or viceversa. For a generic cell with  $N$  nodes, this condition is expressed by

$$f_w(\mathbf{x}^i, \mathbf{x}^f) = \sum_{i=1}^N [m_{i,d}(\mathbf{x}^i)m_{i,s}(\mathbf{x}^f) + m_{i,s}(\mathbf{x}^i)m_{i,d}(\mathbf{x}^f)]. \quad (5)$$

If  $f_w = 0$ , then  $E_w = 0$ ; if  $f_w = 1$ , instead,  $E_w$  depends on fan-in and fan-out conditions, represented by the input slopes  $S_1, \dots, S_n$  and by the output load  $C_L$ . Corresponding to any transition, however, short circuit currents are not influenced by those input (output) parameters associated with input (output) signals that don't change.

Since there are no simple closed-form models for the wasted contribution to power consumption, we approximate  $E_w$  with a first-order function of the I/O parameters:

$$E_w = f_w(c_1 S_1 + \dots + c_n S_n + c_{n+1} f_{out} C_L), \quad (6)$$

where  $f_{out}$  is a Boolean flag taking value 1 corresponding to output transitions ( $f_{out} = out(\mathbf{x}^f) \oplus out(\mathbf{x}^i)$ ), and the input slopes are set to 0 if the corresponding inputs do not change ( $x_i^f = x_i^i \implies S_i = 0$ ). Pattern dependency is thus implicitly accounted for.

Coefficients  $c_1, \dots, c_{n+1}$  are computed with min-square fitting of values obtained by circuit simulation. It is important to notice that the computation of  $E_w$  requires a number of fitting coefficients that is *linear* in the number of inputs and outputs of the cell.

### 3.5 Multiple Transitions

Although the model described above is accurate for perfectly aligned multiple input transitions, this assumption is often violated in practice. In the majority of cases, multiple input transitions are slightly misaligned, possibly by short times (compared to the transition time of the gate). In this case a model that computes the power dissipation observing single input transitions may produce large errors, because it will consider a slightly misaligned multiple transition as a sequence of full transitions.

Assume that a two input transition from input pattern  $\mathbf{x}^i$  to  $\mathbf{x}^f$  is not perfectly aligned. The misalignment causes an intermediate pattern (say,  $\mathbf{x}^m$ ) to appear at the input of the gate for a short period of time. Assume  $\tau$  to be the delay between the misaligned input transitions (*i.e.*, the input *skew*). We call **transient time** the time  $T_{i \rightarrow m}$  needed to reach 90% of the total charge transfer from  $V_{dd}$  to capacitances in the gate (caused by the transition  $\mathbf{x}^i \rightarrow \mathbf{x}^m$ ). There are two limit situations:

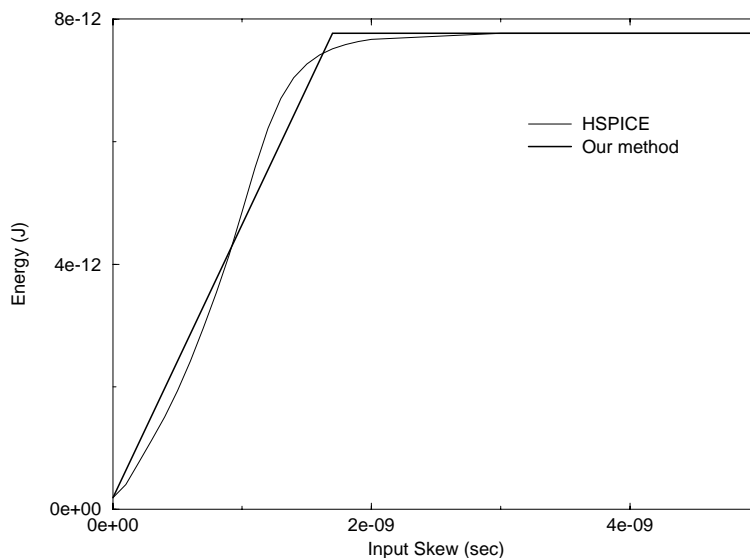


Figure 2: Effect of the input skew on the energy drawn by a three inputs OR gate corresponding to an input transition from  $\mathbf{x}^i = 100$  to  $\mathbf{x}^f = 011$ .

- If  $\tau \ll T_{i \rightarrow m}$ , pattern  $\mathbf{x}^m$  does not appear at the inputs and the energy dissipated is  $E = E_{i \rightarrow f}$ .
- On the other hand, if  $\tau > T_{i \rightarrow m}$ , we have two complete transitions and the total energy dissipation is  $E = E_{i \rightarrow m} + E_{m \rightarrow f}$ .

We approximate the intermediate cases using a linear interpolation between the two limits, as shown in Fig. 2. Namely:

$$E = (E_{i \rightarrow m} + E_{m \rightarrow f}) \frac{\tau}{T_{i \rightarrow m}} + E_{i \rightarrow f} \left(1 - \frac{\tau}{T_{i \rightarrow m}}\right). \quad (7)$$

Clearly this formula holds if  $\tau < T_{i \rightarrow m}$ , while if this is not true we have  $E = E_{i \rightarrow m} + E_{m \rightarrow f}$ .

**Example 7** Consider the OR gate of Fig. 1, and assume that a multiple input transition occurs from  $\mathbf{x}^i = 100$  to  $\mathbf{x}^f = 011$ , with a misalignment ( $\tau$ ) of 1ns between the falling edge of  $x_1$  and the rising edges of  $x_2$  and  $x_3$ . As shown in Fig. 3.a, the input misalignment gives rise to an intermediate input pattern  $\mathbf{x}^m = 000$ . By electrical simulation, the total energy drawn by the cell is of 4.15pJ.

Since the transient time ( $T_{i \rightarrow m} = 1.7\text{ns}$ ) is greater than the input skew ( $\tau = 1\text{ns}$ ), to evaluate  $E$  at logic level we refer to the two limit situations of simultaneous and disjoint input transitions (Figg. 3.b and 3.c), providing:

$$\begin{aligned} E_{i \rightarrow f} &= 0.41\text{pJ}, \\ E_{i \rightarrow m} &= 4.42\text{pJ}, \quad E_{m \rightarrow f} = 3.37\text{pJ}, \end{aligned}$$

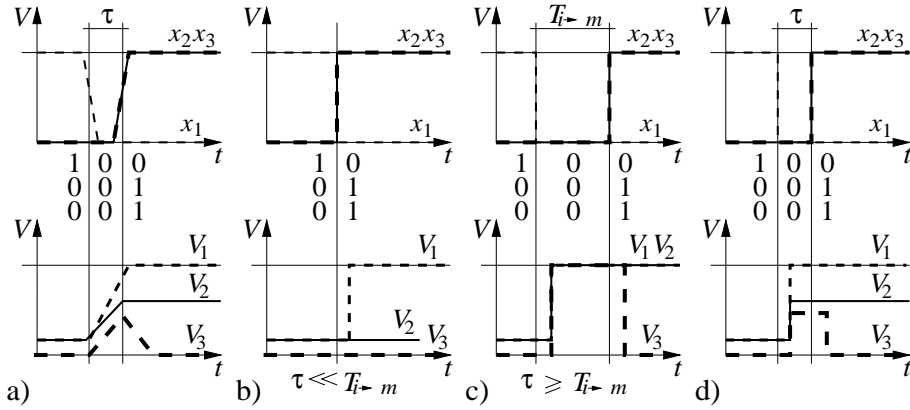


Figure 3: a) Symbolic representation of the effects of a misaligned multiple transition on the internal voltages of the OR gate of Fig. 1. At logic level, we can handle only the two limit situations of b) perfectly aligned input edges, and c) sequences of completely disjoint transitions. However, good estimates of the internal voltages can be obtained in any other case (d) by means of linear interpolation.

respectively. The actual energy estimate is then provided by the following linear interpolation:

$$E = 0.41\left(1 - \frac{1}{1.7}\right) + (4.42 + 3.37)\frac{1}{1.7}pJ = 4.58pJ,$$

with an error of 4.8% from SPICE.  $\square$

The same approach is used to approximate the charge status of the cell at the end of slightly misaligned multiple transitions, as shown in Fig. 3.d.

The linear approximation is obviously exact at the boundaries, but its accuracy depends on the definition of  $T_{i \rightarrow m}$ . In general,  $T_{i \rightarrow m}$  is strongly pattern dependent and it is not equal to the delay used for event propagation. This is shown in the next section.

### 3.6 Timing Information

As mentioned in previous sections, the power drawn by a cell depends not only on the input patterns applied, but also on signal waveforms and arrival times. At the logic level, however, signal slopes are neither represented nor propagated, and simple delay models (such as unit delay) are used for scheduling the events. These approximations have a critical impact on the accuracy of power estimates.

To solve this problem, we provide accurate models of the three main parameters representing the time behavior of each library-cell:

- the propagation delay  $D$  (used by the simulator for the event scheduling),
- the output slope  $S_{out}$  (used for power estimation of the driven gates),
- the transient time  $T$  (used to handle misaligned multiple transitions).



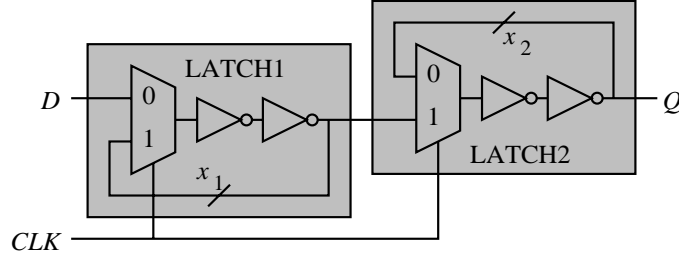


Figure 4: Static implementation of an edge triggered D register composed of two level sensitive latches.

We approximate these parameters with pattern-dependent functions of both the output load ( $C_L$ ) and the average input slope ( $S_{avg}$ ):

$$\begin{aligned}
 D &= c_{0d}(\mathbf{x}) + c_{1d}(\mathbf{x})S_{avg} + c_{2d}(\mathbf{x})C_L; \\
 S_{out} &= c_{0s}(\mathbf{x}) + c_{1s}(\mathbf{x})S_{avg} + c_{2s}(\mathbf{x})C_L; \\
 T &= c_{0t}(\mathbf{x}) + c_{1t}(\mathbf{x})S_{avg} + c_{2t}(\mathbf{x})C_L.
 \end{aligned} \tag{8}$$

The pattern dependent coefficients  $c$  are determined by means of electrical simulations during the library characterization phase: for each final input configuration  $\mathbf{x}^f$  a set of min-square fitting coefficients is obtained.

In principle, we obtain  $2^n$  different values for each coefficient. In practice, however, the majority of them do not change within large sets of input configurations. Hence, the number of possible assignments of the fitting coefficients is usually small and their pattern dependence can be efficiently modeled by means of ADDs [14].

### 3.7 Sequential Elements

In order to describe the model of power consumption in CMOS gates, we have always referred to a static combinational cell (namely, a CMOS implementation of a three input OR gate). In this section we remove this restriction by extending the approach to static and dynamic sequential elements.

#### 3.7.1 Static Sequential Elements

The gate-level representation of a static sequential circuit is always characterized by the presence of feedback signals. Consider the edge triggered register of Fig. 4. At gate level, it can be represented either as a net of six interconnected combinational elements (four inverters and two multiplexers) with two external feedbacks ( $x_1$  and  $x_2$ ), or as a sequence of two latches (LATCH1 and LATCH2) with internal feedback.

In the first case no change is required. Our gate model is directly applied to each component, while feedback signals are explicitly handled by the event scheduling mechanism provided by

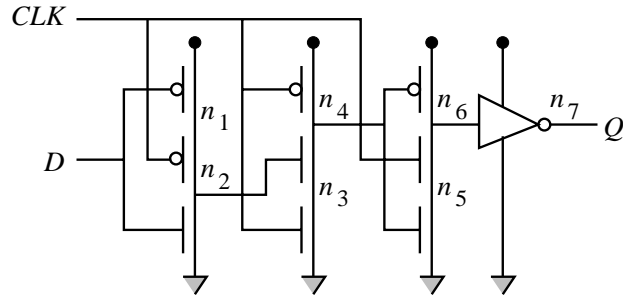


Figure 5: Dynamic CMOS implementation of an edge triggered D register.

the simulation platform (needless to say, the initial state of the sequential elements has to be specified in order to obtain significant simulation results).

In the second case, the whole latches need to be modeled as basic building blocks. We refer to the negative level-sensitive latch of Fig. 4 (namely, LATCH1) with inputs  $D$  and  $CLK$  and output  $x_1$ . Because of the internal feedback, neither the functionality nor the connectivity of the cell (*i.e.*, the values of the connection matrix entries) can be inferred from the knowledge of the current input pattern. Nevertheless, we want to express the connection matrix as a *combinational* function of Boolean variables. To this purpose, the last value of the feedback signal ( $x_1$ ) is to be considered as an additional control variable for the connection matrix:  $\mathcal{M}(D, CLK, x_1)$ .

Notice that  $x_1$  is also the primary output of the cell, and there is a row of the connection matrix associated with it. During simulation, the new value of  $x_1$  is then provided by the model itself. The use of the same signal both as independent and as dependent variable is the implicit representation of the internal feedback.

In general, the connection matrix of a sequential element will be a combinational function of both primary inputs and feedback variables. This is the only extension required to deal with sequential components.

### 3.7.2 Dynamic Elements

Dynamic CMOS logics exploit the memory effects associated with the charge retention at the internal (floating) nodes of a cell. On the other hand, in section 2.1 we remarked that the charge status at the internal nodes of a CMOS cell may have a sizable impact on power consumption. We then constructed a state-dependent symbolic model that takes into account charge retentions at internal nodes. As a consequence, our cell model is inherently able to capture dynamic effects associated with internal parasitic capacitances.

From a structural point of view, the only difference between static and dynamic CMOS logics is that in dynamic logic floating nodes may be used to drive CMOS stages.

**Example 8** Consider for instance the dynamic edge triggered register shown in Fig. 5. The second CMOS stage is driven by internal node  $n_2$ , that is floating when  $D = 0$  and  $CLK = 1$ . In

this case, neither the logic value of  $n_2$  nor the connectivity of the subsequent stage can be inferred from the current values of  $D$  and  $CLK$ . Nevertheless, the charge status at  $n_2$  is provided by our cell model, and the connectivity of the second CMOS stage can be expressed as a combinational function of  $CLK$  and  $n_2$ .  $\square$

In general, to deal with dynamic cells we do not require additional information, but we need to partition the connection matrix and change the sequence of steps involved in model evaluation. In particular, the submatrices associated with cascaded stages must be evaluated in sequence, in order to use partial results to drive the subsequent evaluations.

**Example 9** For instance, the connection matrix of the first stage of the register shown in Fig. 5, is

$$\begin{aligned} m_{1,1} &= 1 & m_{1,2} &= CLK' & m_{1,d} &= D' & m_{1,g} &= CLK'D \\ m_{2,1} &= CLK' & m_{2,2} &= 1 & m_{2,d} &= CLK'D' & m_{2,g} &= D \end{aligned}$$

Whenever an input event occurs, the matrix is evaluated to obtain  $V_{n_2}$  from Eq. (4). Then, the connection matrix of the second stage can be evaluated using  $n_2$  as input variable.

$$\begin{aligned} m_{3,4} &= 1 & m_{3,4} &= n_2 & m_{3,d} &= n_2CLK' & m_{3,g} &= CLK \\ m_{4,3} &= n_2 & m_{4,4} &= 1 & m_{4,d} &= CLK' & m_{4,g} &= n_2CLK \end{aligned}$$

$\square$

In summary, the entries of the connection matrix associated with a generic (combinational or sequential) CMOS cell may be functions of primary inputs, internal variables, and previous values of feedback signals.

### 3.8 Implementation

Routines for both the construction of the connection matrix and the min-square fitting of electrical simulations have been implemented in C using standard packages for BDD and matrix manipulations. VERILOG-XL has been used as simulation platform. The pre-characterized symbolic models of library cells have been written as C functions and made available from logic simulation using the Programming Language Interface (PLI) of VERILOG-XL.

Our simulator has been used as the starting point for the development of PPP, a fully integrated synthesis and simulation environment with short learning curve and architecture-independent Web-based interface. The innovative aspects of the implementation of PPP are described in the next section.

## 4 Web-Based Tool Development

### 4.1 Motivations and Background

The number of tools needed to implement complex systems is ever increasing, and such tools are generally provided by a myriad of suppliers. Integration of EDA tools into unified frameworks

prompts for an increasing effort in the creation of standard interfaces [15, 16]. The definition of standard formats for design descriptions such as VHDL and EDIF has been an important milestone in this direction. However, the user interfaces provided by different EDA vendors still lack in uniformity and compatibility.

Moreover, as computer networking becomes pervasive, design teams will be geographically dispersed, and the need for reliable and straightforward communication paradigms will steadily grow. Computationally demanding tasks (optimization and/or simulation of large circuits) could be performed on high-performance servers remotely connected to the designers by Internet links. Again, a uniform user interface should be provided in this concurrent and distributed engineering environment.

The opportunities for commercial EDA vendors are promising as well. New tool usage paradigms may emerge: users could temporarily connect to a tool provider, perform a specific task and be billed on a usage-time basis. Similarly, demos can be performed across the network, a much more effective form of advertisement, because it gives the perspective user direct hands-on experience. Necessary conditions for such new paradigms to be successful is again the existence of a general and friendly user interface for remote connections and execution control.

The explosive diffusion of an user-friendly and powerful interface such as the World Wide Web [17] (WWW) has prompted several attempts directed to exploit its features in the CAD-EDA area. Virtually every computer user is familiar with the WWW, and Web browsers provide an uniform interface to a number of different communication protocols. A Web-based interface to CAD tools is an important step toward standardization and distributed tool integration. Preliminary results in this direction have been reported in [18] and [19]. In both this works the designer's need for geographically disperse and heterogeneous information is addressed and simple protocols for remote batch execution are described: the user can request services to remote tools, that will perform the required tasks and return the results. The interaction between users and tools is sparse and loose.

Effective execution of remote tools requires a much higher level of interaction: the user should be allowed to change the setting of a parameterized tool run, preview partial result, access visual information like waveforms and network schematics, modify networks and update design databases.

## 4.2 The PPP Paradigm

PPP has been conceived as a modular system composed of interacting tools that may run on different machines and be (possibly) provided by different vendors or contributors. The main target of PPP is the synthesis and the simulation of low-power CMOS circuits, but its modularity allows us to interface with general-purpose commercial and academic tools.

The user accesses PPP using his/her own Web browser, with no additional requirements on hardware or software installation. The tools can reside on remote servers or on the local machine.

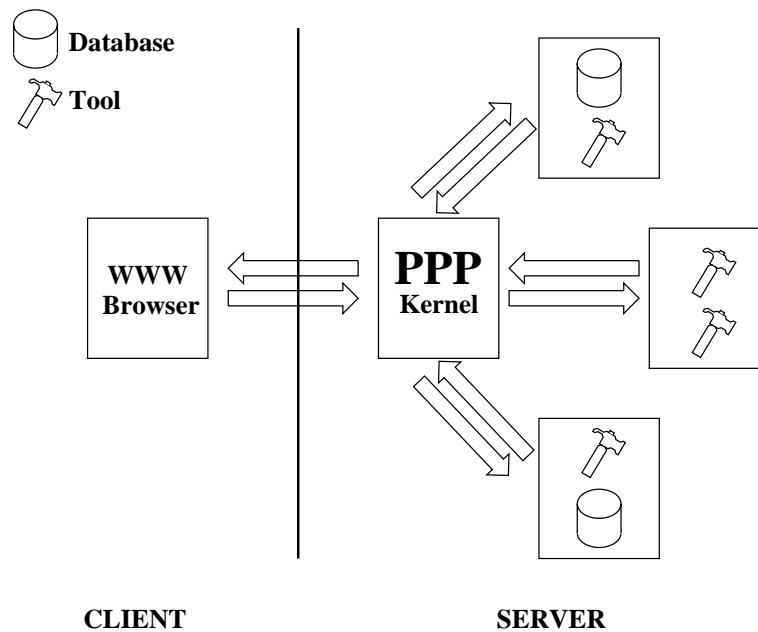


Figure 6: User interaction with PPP

This is fully transparent to the user. The graphical user interface (GUI) of PPP is exactly the same used for Web navigation and no additional effort needs to be spent in familiarizing with a new GUI when the user first accesses the system.

In the design of PPP, we focused on two key ideas: plug-and-play modularity and architecture-independent interactive remote execution. Plug-and-play modularity allows new tools to be integrated in PPP with little effort and no modifications. The impact on other tools already embedded in the environment is negligible. Remote execution can be seen as an advanced caching strategy. Upon invocation, a resource in PPP can maintain its state throughout a sequence of interactions. The state information is not necessarily saved on files to avoid the penalty of iterated disk accesses (or, worse, of sending data across the Internet), but it is kept in memory because the resource does not terminate its execution after every interaction with the user.

From the user's point of view, PPP appears as a remote HTTP server and each user can access it by simply inserting a pointer to the PPP URL in his/her bookmark file. This is the only setup operation required. Figure 6 represents the user interaction with PPP. The rectangles denote different machines connected to the Internet. PPP is the core of a distributed architecture. It manages two different kinds of interface: connection to the client and connection to the resources (tools and databases). The arrows represent Internet protocols (FTP, HTTP, mail, etc).

Multiple users are allowed to concurrently access PPP, similarly to a traditional WWW server. Figure 6 depicts a *centralized* structure. The PPP *kernel* manages all interactions between the users and the tools. In the next section we will describe the organization of the PPP kernel and the overall architecture.

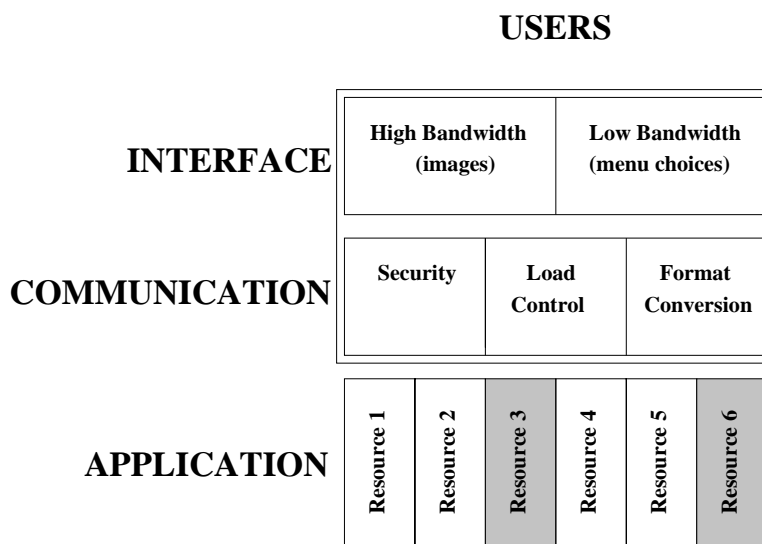


Figure 7: The layered architecture of PPP. Resources represented with shaded rectangles require an high degree of interactivity.

## 5 Tool Architecture

PPP is build upon a layered architecture, following a well-known software engineering paradigm. The three layers are: *application*, *communication* and *interface*. The organization of PPP is shown in Figure 7. The top two layers are embedded in the kernel, while the application layer is distributed. Application is at the bottom of the hierarchy and manages the interaction with the tools and the information sources.

### 5.1 Application Layer

The synthesis and simulation tools embedded in PPP represent the bulk of the application layer and are called *resources*. No constraint is posed on the target architecture and on the programming language used for the implementation of the resources. The resources may run on different machines. Two levels of interaction between resources and the above layers are possible. The simplest interaction is *stateless connection*: the tool performs some manipulation on the input data, produces an output and terminates the execution. Stateless connection is not truly stateless, because the information about previous invocations may be stored in files. Nevertheless, retrieving the state from files imposes heavy performance penalties when highly interactive operation is required (for example, during an user-controlled optimization session). Stateless connection resembles the batch execution features described in [18, 19].

For applications where higher interactivity is required, we provide a novel paradigm called *interactive remote execution*. Once started, the resource does not terminate its execution after every command, but it simply waits for another command to be issued. The resource becomes a *server* that awaits for service requests from the client (the user) keeping complete information

about past requests and their results. Resources that provide interactive remote execution must satisfy some requirements on their external interface. In particular, it must be possible to interactively receive data from another process without terminating the execution. Interactive remote execution is required for running optimization and validation tools that perform user-assisted tasks.

**Example 10** *An application requiring interactive remote execution is logic optimization, where the user can decide among different optimization strategies by observing the quality of intermediate results. In contrast, a long simulation is a typical example of batch execution. After setting up the simulation parameters, the user dispatches the run and does not need to interact with the tool until the run terminates.*

## 5.2 Communication Layer

The communication layer represents the core of the PPP architecture. Its purposes are the following.

- Process users' requests and translate them in a format that is accepted by the resources.
- Collect the results produced by the resources and provide them to the users in a readable/downloadable format.
- Manage data files provided by the users and/or created by the resources and store them where retrieval will be faster.
- Provide security. Different users work on private space and should not be allowed to interact unless they explicitly require to work on a shared design. Access identification should be enforced.
- Manage server's resources. If PPP runs on multiple machines, the communication layer can direct the requests of the users toward unloaded machines.

All functionalities listed above are in some degree implemented in PPP. Each user works in a separate space, where input files and results are stored. User access authentication is enforced by a password mechanism. All format conversions are performed transparently. Since the resources run on different machines, the communication layer must be implemented as a distributed multiprocess application. In the current implementation, scheduling of resources, conflicts and mutual exclusion are managed using simple message files on a shared file system. While this solution is simple and effective, it requires that all machines running resources share a common file system. This requirement may become a limitation and will likely be removed in future versions.

**Example 11** *Format conversion is a typical function performed in the communication layer. For instance, in PPP part of the synthesis process is performed by SIS [20]. The output format provided by SIS is BLIF. The simulation tool encased in PPP (our customized version of Verilog-XL) accepts files in Verilog HDL. The conversion between BLIF and Verilog is performed by a process in the communication layer. The conversion is completely transparent to the user.*

### 5.3 Interface Layer

Interface is the uppermost layer, with which the user interacts. The largest part of the interface layer is directly supported by the WEB browser. If the interaction is limited to simple menu-based communication, the form feature provided by HTML [21] is sufficient. The same holds for small images and graphs. This is however not sufficient. In many cases, the users wants to specify the input or examine the output in more complex ways.

We call *high-bandwidth* the kind of interaction for which the WEB browser does not provide satisfying performance. Examples of high-bandwidth interactions are transfers of large input files (i.e. the networks that the user wants to simulate/optimize) and interactive graphical output (such as waveform or network browsing). In these cases alternate mechanisms for interaction must be provided. For user-originated communication such as the transfer of input files, we currently use the FTP protocol.

For resource-originated communication, such as waveform display, more advanced mechanisms are needed. The resource generates output data files, the communication layer then takes care of transforming the data in a graphical output that is sent to the user. The user can view the graphical output using helper programs or directly through the limited image display capability of the WEB browser.

**Example 12** *After simulation, the users specifies the signals he/she wants to view. This information is communicated to PPP (this is a typical low-bandwidth interaction) using a form. From the simulation output files, the relevant signal transitions are extracted and a waveform image is generated to be sent back to the user. This is a high bandwidth interaction.*

### 5.4 Bandwidth management

A fundamental issue in the design of all layers of PPP is *bandwidth management*. Although local area networks (LAN) can usually provide the bandwidth required for most data transfers, PPP is not limited to run on LANs. When some of the connections are supported by a wide area network (WAN), the bandwidth of the data transfer has to be reduced as much as possible. In the current implementation, the only critical connection is between the PPP kernel and the client. On this connection, bandwidth-critical applications are those involving massive data transfer and a high degree of interactivity. In this case, the level of interaction with the resource is so high that we may want to transfer the resource itself on the client's side.



An example of critical application is waveform display. In the current implementation of PPP, we try to minimize the bandwidth required by sending to the client compressed images of the waveforms. This solution is satisfying only if the user does not need to dynamically update the waveform view very frequently. The advantage of this approach is that the user does not need any dedicated support for waveform display. More aggressive bandwidth reduction can be achieved without requiring the user to install dedicated programs. To this purpose, it is necessary to enable the transmission of executable code across the network. Languages such as JAVA [22] and TCL [23] allow this kind of interaction.

### 5.5 Implementation Details

During a typical user session, PPP appears as a tree of HTML forms that can be navigated by the user. In reality, the HTML pages are *dynamically* created by PERL scripts controlled by the user's commands. The set of PERL scripts that generates the HTML forms for the user is the interface layer of PPP. Although the interaction allowed by HTML forms is limited and not very flexible, the GUI is straightforward and familiar to any user. As a consequence, a completely inexperienced user can obtain results after a single PPP session.

The communication layer is composed by another set of PERL scripts. The user does not directly access the communication layer, but its commands are parsed by the scripts in the interface layer, translated, and sent to the communication layer. The scripts in the communication layers perform mainly translation and setup tasks to prepare the environment needed for tool execution. Another important function performed in the communication layer is the choice of the machine on which the requested tool will run.

Finally, the environment is ready for the execution of the tools. Tool execution is managed by the application layer. If basic batch runs are requested, the tool is simply executed with the input information provided by the communication layer. Tools that execute in batch mode can be incorporated in PPP with minimal effort: the interface and communication layers are modified to allow the user to access the tool and to provide the files needed for the batch run.

When interactive remote execution is required, the process of linking the tool to PPP is less straightforward. The standard input and output channels must be re-directed to a script that manages the interaction with the interface layer. The script is run when the user specifies a command, it translates the input format and it sends the command to the tool. The script then waits for the results of the command to be sent back by the tool. The results are saved on files or sent directly to the user after being translated to HTML. Finally the script terminates the execution, closing the contact with the tool and the interface layer. Notice that the tool *does not terminate the execution*, thus the state of the program remains in the main memory until the user explicitly asks to terminate the session. Whenever a new command is issued by the user, the interaction with the tool is managed by a new run of the communication script.

Setting a tool for interactive remote execution requires i) the ability of redirecting the stan-

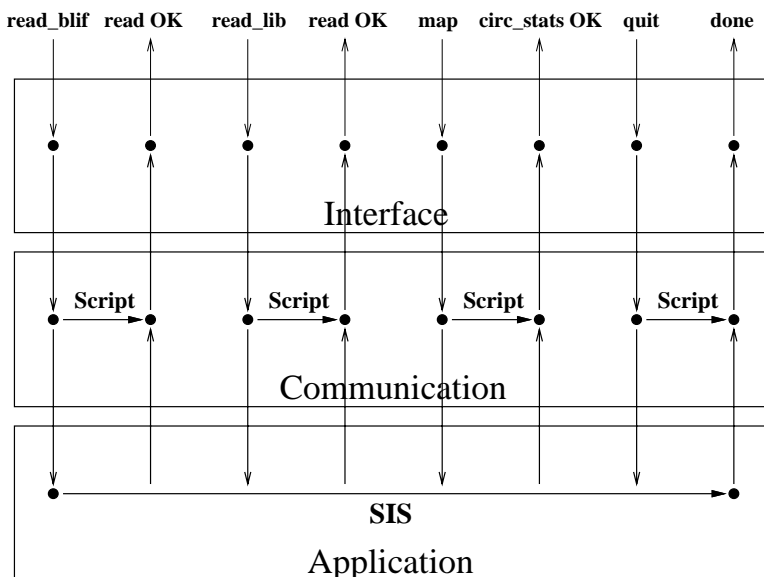


Figure 8: An example of interactive remote execution: SIS session

standard input and output of the tool, ii) the implementation of the communication script with the characteristics described above. In the current implementation of PPP, interactive remote execution is available for SIS.

**Example 13** In Figure 8 we show a diagram representing multiple commands during a SIS session performed with the interactive remote execution paradigm. Time proceeds from left to right. Arrows represent the duration of processes. Dots represent their start and termination points.

When the user issues a command a process in the interface layer is started to translate the command in the format required by SIS (the duration of this process is very short, therefore it is represented as a single dot). In the communication layer a process is started (with the label *Script*) to manage the interaction between SIS and the user. The command is then passed to SIS. When SIS returns the result the script will pass it to the interface layer that will translate it to *HTML* and serve it to the users. Then the communication process terminates, but the execution of SIS does not terminate until the user issues the *quit* command.

## 6 PPP User Session

To give a more concrete understanding of the features provided by PPP, we describe a simulation session.

User identification is enforced to access PPP. The access point is an *HTML* form asking for user's name, password and e-mail address. When the form is applied, the main menu of PPP appears and two directories are created on the server file-system to allow the user to work in

a private space: an I/O directory that can be accessed from the client for explicit file transfers based on FTP, and a (hidden) work directory used by the system to store intermediate results.

Three sets of interacting tools can be accessed from the main page of PPP: circuit optimization and mapping, test sequence specification and power simulation. All these tools are embedded into a unified framework that hides to the user the details of their interaction. A typical user session consists of visiting all the three environments, possibly iteratively, directly from the Web-browser. Partial results are always available and visible from any tool. The (partial) result of a synthesis session is taken as the default circuit for simulation, and its inputs are the default signals handled by the pattern generation tools. In the following we describe step by step a simulation session.

## 6.1 Circuit Specification and Mapping

Since the simulation engine of PPP is a cell-based gate-level simulator, the circuit to be simulated is first mapped onto a pre-characterized cell library. This is done using the circuit specification form, that is directly accessible from the main page. Three fields need to be specified: *i*) the name of the file containing the circuit description (*slif*, *blif* and *verilog* are supported), *ii*) the name of a pre-characterized cell library, and *iii*) the optimization options that will be used during the mapping. The circuit is read from the user I/O directory, where the user can put his/her own circuits using a standard file transfer protocol. Notice that the user I/O directory will not be removed at the end of the simulation session. The user can retrieve his/her own files whenever he/she accesses PPP. To avoid excessive disk usage on the server, a hard limit is put on the amount of space available to each user. Moreover, unused I/O directories are deleted after a few days.

The cell library has to be selected by the user. At the moment only one library has been characterized, but future releases will allow the user to automatically characterize his/her own library according to the cell model described in section 3. Optimization options can also be specified for the mapping, and a batch run of logic optimization and library binding is run. A form-based menu is available to select the optimization options. When applying the form, SIS [20] is remotely run to map the circuit onto the library. The mapped circuit is then stored into a new file in the user's I/O directory and it is taken as default circuit for simulation. Since PPP uses Verilog-XL as simulation platform, a Verilog description of the mapped circuit is also created and stored in the work directory. Circuit statistics are available at any time in terms of input, output and gate counts, number of state variables and library cells used.

Alternatively, the user can start an interactive optimization session. If this option is selected, a command prompt is displayed. The user issues optimization commands at the prompt, the synthesis tool executes them and reports to the user. Notice that the interactive optimization session is an example of a tighter interaction level than that allowed by batch run. Between two consecutive optimization commands, the synthesis tool *does not terminate execution*, thus

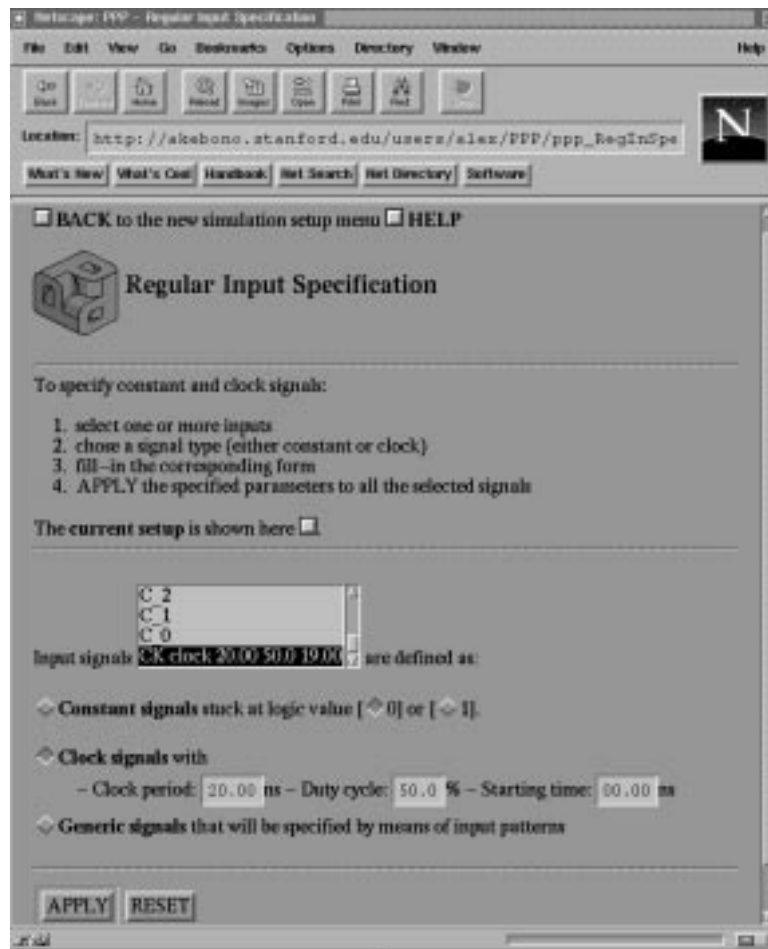


Figure 9: User interaction with PPP: simulation setup

the structure of the network is kept in the memory of the machine running the tool. For large networks, this kind of interaction is paramount to obtain acceptable latency between two successive user commands.

After optimization and mapping, the circuit is ready to be simulated with a default test sequence of 100 random test vectors applied with a 20ns time period. To specify a different simulation setup, test-synthesis tools are provided. They can be accessed by choosing the simulation-setup entry of the main menu.

## 6.2 Simulation Setup

The simulation setup can be either read from a file in the user's I/O directory or specified using the interactive interface of PPP. In this case, three main HTML forms are available to specify: *i*) global parameters, *ii*) constant and clock signals and *iii*) generic inputs. Global parameters include the simulation style (either random or deterministic), the test size and the time step between input patterns.

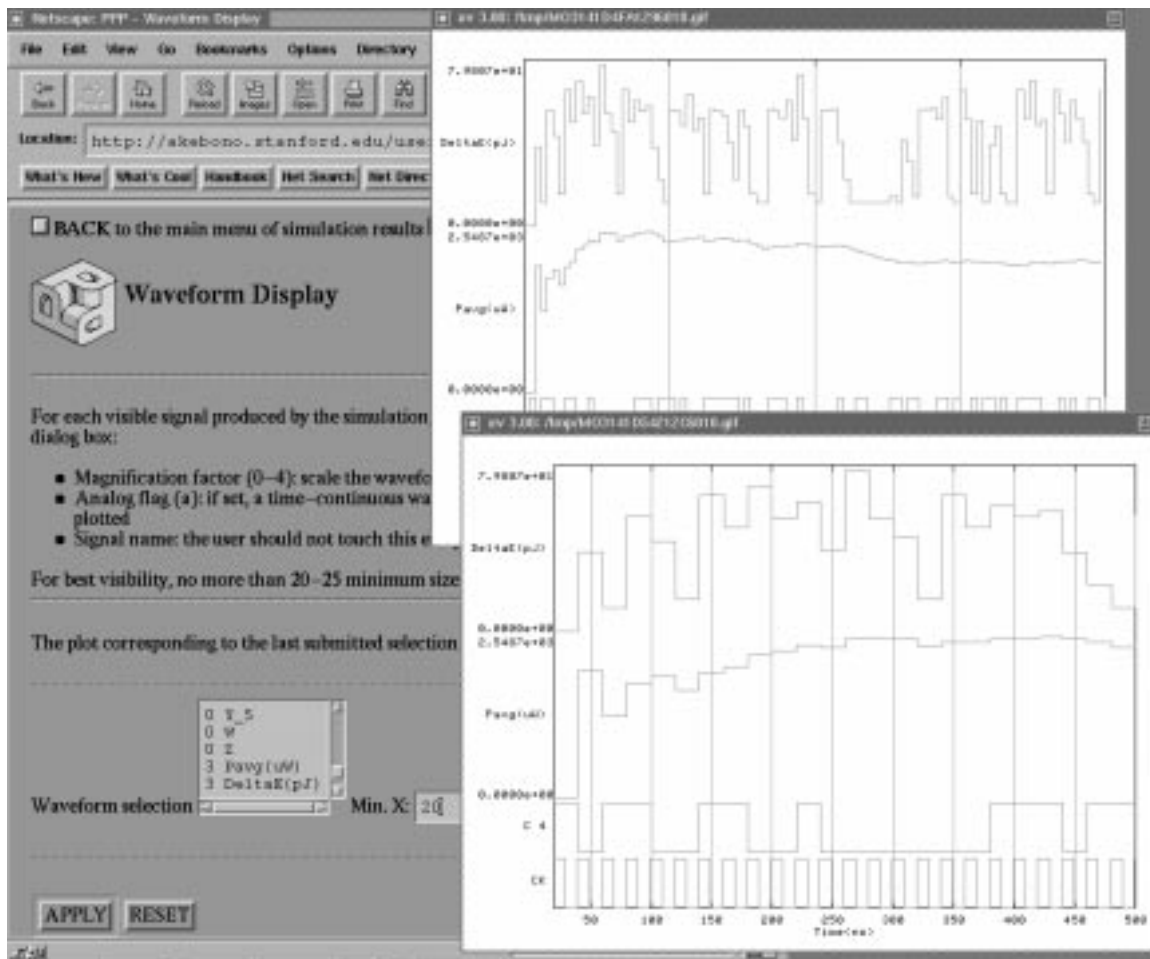


Figure 10: User interaction with PPP: waveform display

The constant and clock signals specification form (Fig. 9) allows the user to specify some signals (selected among the list of current circuit inputs) to behave either as a periodic waveform or as a constant. In the first case clock period, duty cycle and skew can be arbitrarily set. In the second case a logic value is to be specified. Specifications are applied to the selected signals whenever the form is submitted.

Similar forms are available to specify input signals that will not have a square or constant behavior. In deterministic simulation, these signals will be set to 0 by default, but an arbitrary test sequence can be either read from a file or interactively specified. In random simulation, 50% signal and transition probabilities are used by default to generate random test sequences, but different values can be assigned. At any time, the current simulation setup can be analyzed, modified, or saved in a file for later re-use.

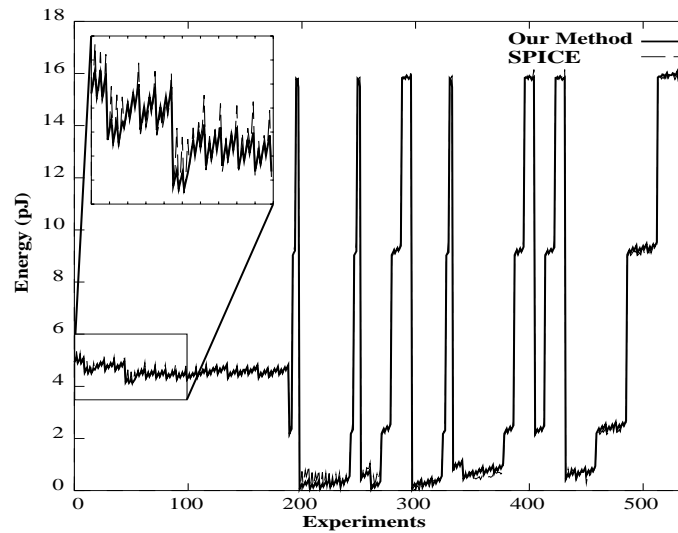


Figure 11: Accuracy from SPICE of our model of a three input OR gate. Results refer to a set of 540 experiments obtained by applying to the cell all possible input pairs, and by varying fanin and fanout conditions in a wide range of realistic values.

### 6.3 Power Simulation

The PPP simulator is accessed by choosing the power simulation option of the main menu. From the first page of the simulation interface the user is allowed to: *i*) look at the circuit statistics, *ii*) look at the current simulation setup, *iii*) run the simulator by applying the current simulation setup to the current circuit, and *iv*) analyze the results of the last simulation run.

A simulation run consists of a remote execution of our simulator and causes the updating of simulation results. CPU and memory consumptions are reported at the end of each simulation run.

There are two sets of simulation results: time-domain waveforms and statistical analysis. The Web-based waveform display is shown in Fig. 10. It consists of a HTML form that allows the user to select the signals to be displayed among the list of all available data. Both Boolean signals (inputs, outputs, clocks and state variables) and analog waveforms (supply energy and power) can be displayed. A signal is selected by specifying its scale factor (*i.e.*, its vertical magnification) to be different than 0 (that is the default value). The time range can also be specified. When the form is applied, data are processed, the waveform plot is saved in a GIF file and a hyperlink is created to access the GIF file from the Web-browser. Fig. 10 shows the result of two subsequent applications of the interface form on the same set of data (namely the results of a PPP simulation of sequential benchmark S208). Two Boolean signals (clock CK and input C4) and two analog waveforms (the partial estimate for the average power and the supply energy drawn by the circuit for each input pattern) are displayed together for different time ranges.

benchmark		test	HSPICE			PPP			error
name	gates	length	P(mW)	CPU(s)	RAM	P(mW)	CPU(s)	RAM	%
C17	6	100	<b>0.435</b>	62.4	0.2M	<b>0.432</b>	0.5	0.2M	0.7
C432	215	100	<b>11.510</b>	3120.0	3.0M	<b>10.954</b>	13.0	1.5M	4.8
C499	496	100	<b>21.926</b>	7276.2	6.2M	<b>22.884</b>	32.7	3.2M	4.1
C880	342	60	<b>16.262</b>	2881.7	4.8M	<b>16.405</b>	13.9	2.3M	0.9
C1355	584	50	<b>23.689</b>	4076.6	7.1M	<b>24.101</b>	18.4	3.8M	1.7
C1908	602	50	<b>33.018</b>	5841.5	8.2M	<b>33.920</b>	22.4	3.9M	2.7
C3540	1165	50	–	–	–	<b>71.250</b>	59.2	7.7M	–
C5315	1877	100	–	–	–	<b>130.413</b>	165.3	12.4M	–
C7552	2892	100	–	–	–	<b>222.823</b>	272.7	18.3M	–
cmb	50	100	<b>1.305</b>	444.9	0.8M	<b>1.329</b>	2.7	0.4M	1.8
decod	54	100	<b>1.385</b>	412.7	0.7M	<b>1.400</b>	2.7	0.4M	1.1
parity	75	100	<b>2.381</b>	591.4	1.0M	<b>2.302</b>	3.6	0.6M	3.4
pcler8	80	100	<b>2.959</b>	742.5	1.3M	<b>3.028</b>	3.3	0.6M	2.3
count	113	100	<b>4.985</b>	1290.9	1.9M	<b>5.081</b>	5.9	0.9M	1.9
comp	163	100	<b>6.700</b>	1698.6	2.1M	<b>6.832</b>	9.6	1.1M	1.9
b9	121	100	<b>4.822</b>	1206.9	1.8M	<b>4.755</b>	6.6	0.9M	1.4
frg1	124	100	<b>4.934</b>	1316.6	1.8M	<b>4.957</b>	7.5	0.9M	0.5
x1	345	100	<b>13.660</b>	4439.7	4.8M	<b>13.336</b>	20.5	2.4M	2.4
x4	487	100	<b>26.698</b>	4445.2	6.7M	<b>25.549</b>	26.0	3.3M	4.3
alu2	359	50	<b>17.881</b>	3362.6	5.5M	<b>18.550</b>	12.4	2.4M	3.6
alu4	716	50	<b>31.565</b>	14765.9	12.2M	<b>32.878</b>	22.9	4.7M	4.0
frg2	1253	50	–	–	–	<b>57.746</b>	35.0	8.5M	–
k2	1943	100	–	–	–	<b>51.742</b>	73.9	13.4M	–

Table 1: Experimental results on combinational benchmark circuits. Data refer to sequences of random generated test-vectors with 20ns clock periods (missing results mean that the corresponding simulation exceeded 10 hours of CPU and/or 20 Mbytes of RAM).

A similar interface is available for statistical results. In particular, statistical data are collected about the local average power consumption (*i.e.*, the power consumption of each cell) and the total energy drawn by the circuit corresponding to each input transition. Statistical results are shown in terms of standard deviation and minimum, maximum and mean values. Moreover, plots of the probability distributions are remotely generated and made accessible to the user by means of hyperlinks.

## 7 Experimental Results

We have tested PPP using a low-power CMOS [24] library (including complex gates, two-level

benchmark			test length	HSPICE			PPP			error %
name	gates	FFs		P(mW)	CPU(s)	RAM	P(mW)	CPU(s)	RAM	
S27	12	3	100	<b>0.600</b>	316.0	0.4M	<b>0.601</b>	3.5	0.2M	0.2
S208	72	8	100	<b>2.097</b>	3692.8	1.5M	<b>2.100</b>	8.2	0.6M	0.1
S953	342	29	100	<b>8.768</b>	27083.6	7.6M	<b>8.310</b>	36.2	2.6M	5.2
S1196	466	18	50	<b>15.918</b>	18534.6	7.6M	<b>15.775</b>	33.6	3.4M	0.9
S1238	522	18	100	–	–	–	<b>17.953</b>	74.8	3.8M	–
S5378	1346	163	100	–	–	–	<b>35.934</b>	157.8	10.5M	–

Table 2: Experimental results on sequential benchmark circuits. Data refer to sequences of random generated test-vectors with 20ns clock periods (missing results mean that the corresponding simulation exceeded 10 hours of CPU and/or 20 Mbytes of RAM).

cells and dynamic elements). Each library cell has been characterized as described in Section 2, using HSPICE [25] to perform electrical simulations.

To verify the single-pattern accuracy of models provided by the characterization process, we have tested each library cell for all possible test-pairs and for a wide range of fanin and fanout conditions. In the worst case, the average absolute error from HSPICE has been of 4% of the average estimated power, with a standard deviation of 0.2%. Fig. 11 reports the results of the whole set of experiments run to verify the model of a three input OR gate.

The same accuracy has been obtained by applying to each cell a sequence of 100 randomly generated test vectors with 50% of misaligned multiple input transitions.

At last, we have simulated several (combinational and sequential) circuits obtained by mapping a large set of well known benchmark circuits on our test library. Circuits have been simulated by applying randomly generated sequences of input patterns with a clock period of 20ns. Experimental results on combinational and sequential circuits are reported in Tables 1 and 2 respectively: for some circuits the power consumption provided by HSPICE has been overestimated by PPP, while for some other circuits it has been underestimated. In particular, the worst case error has been the underestimation of 4.8% of the power consumption of C432. Fig. 12 shows the convergence of the average power estimate during a random simulation of sequential circuit S344.

As concerns performance, the CPU times taken on a Sun SPARCstation IPX show that PPP is up to three orders of magnitude faster than HSPICE. On the other hand, the performance loss with respect to simple VERILOG simulations based on transition counts with unit delay models is within a factor of 6.

For circuit C17, local power estimates are also reported in Table 3. It is worth noting that the average power drawn by each internal gate has been estimated with a worst case accuracy of 6% from HSPICE.



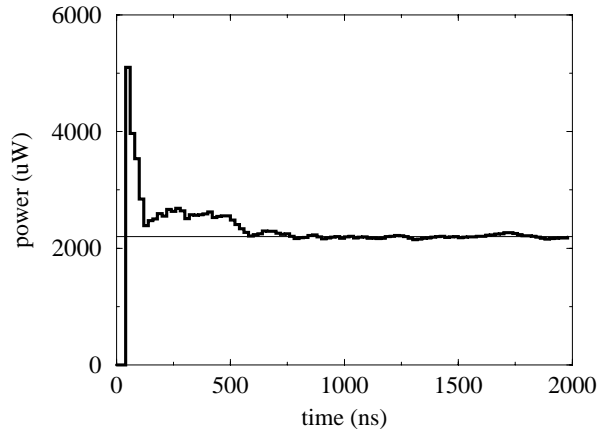


Figure 12: Convergence of the average power estimation during a random simulation of circuit S208 with 100 test patterns. A 20ns clock period has been used.

## 8 Conclusions and Future Work

In this work we presented a cell characterization and logic simulation algorithm that reduces the gap between the accuracy of electrical and logic-level power estimation for cell-based designs. Statistical uncertainties on device characteristics or inaccuracies on wiring capacitance extraction and modeling may lead to mismatches between circuit simulation and measured values that are larger than the inaccuracy of our simulator. As a consequence, our simulation technique gives the designer a level of confidence on power dissipation estimates comparable to those attainable with computationally expensive circuit simulation. The high local accuracy makes our tool a valuable source of information for power optimization algorithms that operate locally within a gate-level network.

Our technique achieves better accuracy than previously presented approaches and requires storage of lookup tables with size similar to those required for logic simulation with accurate delay. Important effects such as charge sharing, short circuit current, and misaligned multiple input transitions are taken into account. Moreover, we use as simulation platform a well known VERILOG simulator such as VERILOG-XL, making the interface with pre-existing design flows and RTL simulation completely straightforward.

The customized Verilog simulator has been embedded in PPP, an integrated Web-based environment for the simulation of low-power VLSI systems. We have described the architecture and the implementation of PPP. We believe that PPP is an example of a new paradigm for distributed network-based applications, where the connectivity offered by Internet is exploited not only for retrieving information but also to dispatch and control execution.

On-going work is focused on integrating more advanced functionalities in PPP. New algorithms for behavioral power estimation will be included in future versions of the tool. Moreover,

Cell #	Power (mW)		Error	
	HSPICE	PPP	(mW)	(%)
0	0.032	0.031	-0.001	3
1	0.038	0.037	-0.001	3
2	0.043	0.042	-0.001	2
3	0.156	0.154	-0.002	1
4	0.032	0.030	-0.002	6
5	0.134	0.138	+0.004	3
tot	0.435	0.432	-0.003	1

Table 3: Local power consumption of a NAND-only realization of benchmark circuit *C17*. Data refer to a sequence of 100 random generated test vectors, with a 20ns clock period.

we are currently developing algorithms that will allow accurate estimation of current waveforms at the logic level. Synthesis tools for low-power will be integrated in PPP as well. In summary, the implementation of PPP demonstrates the feasibility of one key concept: a uniform user interface for a heterogeneous set of EDA tools based on the WWW.

## 9 Acknowledgements

We would like to thank Michele Favalli at DEIS, University of Bologna, for many useful suggestions.

## References

- [1] C. Huang, B. Zhang, *et al.*, "The design and implementation of Powermill," in *Proc. of IEEE Symp. on Low Power Electronics*, pp. 105–110, 1995.
- [2] F. Najm, "A survey of power estimation techniques in VLSI circuits," *IEEE Transaction on VLSI Systems*, vol. 2, no. 4, pp. 446–455, 1994.
- [3] C. Y. Tsui, M. Pedram, and A. Despain, "Efficient Estimation of Dynamic Power Dissipation under a Real Delay Model," in *Proc. of IEEE Intl Conf. On Computer Aided Design*, pp. 224–228, 1993.
- [4] R. Marculescu, D. Marculescu, and M. Pedram, "Logic level power estimation considering spatiotemporal correlations," in *Proc. of IEEE Intl Conf. On Computer Design*, pp. 294–299, 1994.
- [5] D. Liu and C. Svensson, "Power consumption estimation in CMOS VLSI chips," *IEEE J. of Solid State Circuit*, vol. 29, no. 6, pp. 663–670, 1994.
- [6] P. Landman and J. Rabaey, "Architectural power analysis, the Dual Bit Type method," *IEEE Transaction on VLSI Systems*, vol. 3, no. 2, pp. 173–187, 1995.
- [7] R. S. Martin and J. Knight, "Power-Profiler: optimizing ASICs power consumption at the behavioral level," in *Proc. of Design Automation Conf.*, pp. 42–47, 1995.
- [8] B. J. George *et al.*, "Power analysis and characterization for semi-custom desing," in *Proc. of Intl Workshop on Low Power Design*, pp. 215–218, 1994.
- [9] J.-Y. Lin *et al.*, "A cell-based power estimation in CMOS combinational circuits," in *Proc. of IEEE Intl Conf. On Computer Aided Design*, pp. 304–309, 1994.
- [10] H. Sarin and A. McNelly, "A power modeling and characterization method for logic simulation," in *Proc. of IEEE Custom Integrated Circuits Conference*, pp. 363–366, 1995.
- [11] L. Benini, M. Favalli, and B. Riccò, "Analysis of hazard contribution to power dissipation in CMOS IC's," in *Proc. of Intl Workshop on Low Power Design*, pp. 27–32, 1994.
- [12] R. E. Bryant, "Graph-based algorithms for boolean function manipulation," *IEEE Transaction on Computers*, vol. 35, no. 8, pp. 677 – 691, 1986.
- [13] N. Weste and K. Eshraghian, *Principles of CMOS VLSI Design (Second Edition)*. Addison-Wesley, 1992.
- [14] R. Bahar *et al.*, "Algebraic decision diagrams and their applications," in *Proc. of IEEE Intl Conf. On Computer Aided Design*, pp. 188–191, 1993.
- [15] T. J. Barnes *et al.*, *Electronic CAD frameworks*. Kluwer Academic Publishers, 1992.
- [16] A. Bededenfeld and R. Camposano, "Tool integration and construction using generated graph-based design representation," in *Proc. of Design Automation Conf.*, pp. 94–99, 1995.
- [17] T. Berners-Lee *et al.*, "The world-wide web," *Communications of the ACM*, vol. 37, no. 8, pp. 76 – 82, 1994.
- [18] M. J. Silva and R. H. Katz, "The case for design using the World Wide Web," in *Proc. of Design Automation Conf.*, pp. 579–585, 1995.
- [19] P. G. Ploger *et al.*, "WWW Based structuring of codesigns," in *Proc. of Intl Symposium on System Synthesis*, pp. 138–143, 1995.
- [20] E. Sentovich *et al.*, "Sequential circuit design using synthesis and optimization," in *Proc. of IEEE Intl Conf. On Computer Design*, pp. 328–333, 1992.
- [21] "HyperText Markup Language (HTML)," *Working and background materials*, <http://www.w3.org/hypertext/WWW/MarkUp/MarkUp.html>.

- [22] Sun Microsystems, "The JAVA language environment: a white paper," <http://java.sun.com/whitePaper/java-whitepaper-1.html>.
- [23] J. K. Ousterhout, *Tcl and the Tk toolkit*. Addison-Wesley, 1994.
- [24] T. Burd, "Current Estimation in MOS IC Logic Circuits," in *M. S. Report UC Berkeley*, UCB/ERLM94/89.
- [25] *HSPICE User's Manual*. Meta-Software Inc., Campbell-CA.